



OPEN

Unconventional critical behaviour in weak ferromagnets $\text{Fe}_{2-x}\text{Mn}_x\text{CrAl}$ ($0 \leq x < 1$)

Kavita Yadav, Dheeraj Ranaut & K. Mukherjee

Recent investigation on weak ferromagnets $\text{Fe}_{2-x}\text{Mn}_x\text{CrAl}$ ($0 \leq x < 1$) reveal the existence of a cluster glass phase (CGP) and a Griffiths-like phase (GP) below and above the ferromagnetic transition temperature (T_C), respectively [(2019) *Sci. Rep.* 9 15888]. In this work, the influence of these inhomogeneous phases on the critical behaviour (around T_C) of the above-mentioned series of alloys has been investigated in detail. For the parent alloy Fe_2CrAl , the critical exponent γ is estimated as ~ 1.34 , which lies near to the ordered 3D Heisenberg class, whereas the obtained value of the critical exponent $\beta \sim 0.273$ does not belong to any universality class. With increment in Mn concentration, both exponents γ and β increase, where γ and β approach the disordered and ordered 3D Heisenberg class, respectively. The observed deviation of γ and unconventional value of δ can be ascribed to the increment of GP with Mn-concentration. The trend noted for β can be attributed to the increment in CGP regime with an increase in Mn-content. The estimated critical exponents are consistent and reliable as corroborated using the scaling law and equations of state. Our studies indicate that the critical phenomenon of $\text{Fe}_{2-x}\text{Mn}_x\text{CrAl}$ ($0 \leq x < 1$) alloys possibly belong to a separate class, which is not described within the framework of any existing universal model.

In the last couple of decades, the family of Heusler alloys has been extensively investigated due to novel magnetic phases like ferromagnetic, helimagnetic, Pauli paramagnetic and heavy fermionic^{1–4} exhibited by them. Interestingly, the majority of the Heusler alloys undergoes ferromagnetic transitions and tends to saturate in weak magnetic field⁵. This long-range ordering gets significantly modified by various substitutions, anti-site disorder, and variations in stoichiometry. For example, in $\text{Fe}_2\text{V}_{1-x}\text{Cr}_x\text{Al}$ alloys, the substitution of Cr at the V site alters the magnetic interactions between the clusters. This alternation leads to the evolution of FM ordering in this series of alloys⁶. In $\text{Fe}_2\text{Cr}_{1-x}\text{Mo}_x\text{Al}$ series of alloys, with Mo substitution, a significant decrement in value of the ferromagnetic transition temperature (T_C) is noted⁷. In this context, analysis of critical exponent is useful to understand the role of a substitution, structural disorder, or stoichiometric variations in alteration of the FM interactions. This process has also been followed to investigate the phase transition (second order) in the Heusler alloys^{7–17}. For instance, Phan et al.⁸ showed that Sn substitution at Mn site in $\text{Ni}_{50}\text{Mn}_{50-x}\text{Sn}_x$ affects the short-range FM interactions and lead to the formation of ordered FM phase in the system. Additionally, the role of various substitutions is studied through critical exponent analysis as reported in $\text{Ni}_{43}\text{Mn}_{46}\text{Sn}_8\text{Z}_3$ ($Z = \text{Cr}$ and In), $\text{Ni}_{47}\text{Mn}_{40}\text{Sn}_{13-x}\text{Cu}_x$, $\text{Ni}_{22}\text{Mn}_{0.72-x}\text{V}_x\text{Ga}_{1.08}$ ^{10–12}. Furthermore, disorder also influences the critical phenomenon around FM transition^{9,18–20}. In $\text{Pr}_{0.5}\text{Sr}_{0.5-x}\text{Ag}_x\text{MnO}_3$, it is reported that the obtained critical exponents do not belong to any conventional universal class. The increment in Ag concentration leads to an augmentation in anti-site disorder which results in the short-range interaction in the system²⁰. In $\text{Ni}_{50}\text{Mn}_{37}\text{Sn}_{13}$, it is observed that Gd substitution at Ni site results in the formation of long-range FM ordering⁹. Presence of disorder in transition metal-based oxide systems can lead to the formation of GP. This phase affects the long-range ordering in these systems and unconventional critical exponents are reported^{21,22}. However, the effect of GP on critical exponents is still poorly understood in the Heusler alloys.

Recently, we have reported the physical properties of $\text{Fe}_{2-x}\text{Mn}_x\text{CrAl}$ ($0 \leq x \leq 1$) Heusler alloys²³. Our results reveal that parent alloy Fe_2CrAl undergoes from FM to paramagnetic (PM) transition near $T_C \sim 202$ K. It exhibits cluster glass phase (CGP) below $T_{f1} \sim 3.9$ K and GP above $T^* \sim 300$ K. It is observed that with Mn substitution (as $x \rightarrow 1$) T_C shifts significantly towards lower temperature, with complete disappearance of FM behaviour in FeMnCrAl . Additionally, the alloys show CGP at low temperatures. Also, GP is found to be persistent in all alloys, with a decrement in T^* with Mn concentration. Hence, it is of interest to investigate: (a) how increment of Mn content at Fe site in Fe_2CrAl and presence of CGP influence the critical phenomena and FM interactions near T_C

School of Basic Sciences, Indian Institute of Technology, Mandi, Himachal Pradesh 175005, India. email: kaustav@iitmandi.ac.in

and (2) whether the existence of GP is always a precursor to the observed divergence in critical exponents values from the values noted in universality model. Hence, to study the aforementioned questions, in this manuscript we have investigated the critical behaviour of $\text{Fe}_{2-x}\text{Mn}_x\text{CrAl}$ ($0 \leq x < 1$) Heusler alloys in the vicinity of T_C .

Results

In order to analyse the critical phenomenon near T_C , where a magnetic material undergoes a second order phase transition (SOPT) from PM state to FM state, various critical exponents are determined. In SOPT, spontaneous magnetization $M_S(T)$ (below T_C), initial inverse susceptibility $\chi_0^{-1}(T)$ (above T_C) and magnetization M at T_C are related to each other by the following power-law equations²⁴:

$$M_S(T) = A(-\varepsilon)^\beta, \varepsilon < 0 \quad (1)$$

$$\chi_0^{-1}(T) = B(-\varepsilon)^\gamma, \varepsilon > 0 \quad (2)$$

$$M = CH^{\frac{1}{\delta}}, \varepsilon = 0 \quad (3)$$

where γ , β and δ are the value of critical exponents; A, B, and C are the constants; and $\varepsilon = (T - T_C)/T_C$ is the reduced temperature. From the scaling hypothesis, the relationship among $M(H, \varepsilon)$, H , and T is expressed as

$$M(H, \varepsilon) = \varepsilon^\beta g_\pm \left(\frac{H}{\varepsilon^{\beta+\gamma}} \right) \quad (4)$$

where $g_-(T < T_C)$ and $g_+(T > T_C)$ are regular functions²⁰. The Eq. (4) can be re-written as:

$$m = g_\pm(h) \quad (5)$$

where $m = \varepsilon^{-\beta} M(H, \varepsilon)$ and $h = \varepsilon^{-(\beta+\gamma)} H$ (m = renormalized magnetization, h = renormalized magnetic field). The above equation signifies that in case of correct choice of critical exponents and scaling relations, two separate universal curves (one below and one above T_C) will be noted. This criterion is essential for validity of critical region²⁰. It is also noted that the exponents lying in the asymptotic region ($\varepsilon \rightarrow 0$) show universal behaviour. But the exponents often exhibit methodical trends or crossover phenomena when T_C is approached^{25,26}. This appears when there is existence of disorder or couplings in the system. Due to this reason, the temperature dependent effective critical parameters (for $\varepsilon \neq 0$) are introduced. These effective parameters show non-universal behaviour, and are given by:

$$\beta_{\text{eff}} = \frac{d[\ln M_S(\varepsilon)]}{d(\ln \varepsilon)}, \gamma_{\text{eff}} = \frac{d[\ln \chi_0^{-1}(\varepsilon)]}{d(\ln \varepsilon)} \quad (6)$$

These exponents should approach universal behaviour in the asymptotic limit^{25,26}.

Conventionally, Arrott plots are used to analyse the critical region around T_C . In this method, the isotherms are represented in the form of M^2 vs H/M , which forms a set of parallel straight lines about T_C ²⁷. This plot follows the mean field model ($\beta = 0.5$, $\gamma = 1$) and isotherms exhibit linear behaviour in the high field region. It also provides us the magnitude of the $M_S(T)$ and $\chi_0^{-1}(T)$ as an intercept on M^2 and H/M axis, respectively. Arrott plot for all the alloys is plotted around T_C (shown in supplementary material Fig. S1a–d). For all the alloys, it is observed that all the curves in the plot exhibit non-linear downward curvature in the high field regime. This indicates that the critical behaviour of $\text{Fe}_{2-x}\text{Mn}_x\text{CrAl}$ ($0 \leq x < 1$) alloys cannot be described based on the mean field theory. Moreover, according to Banerjee criterion the downward curvature signifies the second order nature of the phase transition²⁸. A generalized form of this analysis, known as Modified Arrott plot (MAP) involves plotting $M^{1/\beta}$ vs $H/M^{1/\gamma}$ in the critical regime. It is given by:

$$\left(\frac{H}{M} \right)^{\frac{1}{\gamma}} = X \left(\frac{T - T_C}{T} \right) + YM^{\frac{1}{\beta}} \quad (7)$$

where X and Y are the constants²⁹. However, determination of critical exponents through this method is a non-trivial task as β and γ are two variable parameters involved in Eq. (7). This can lead to significant errors in the obtained value of exponents. Hence, for the appropriate selection of β and γ an iterative method has as suggested by Arrott et al.²⁹. Therefore, to start this process, initial values of critical exponents are taken as $\beta = 0.365$ and $\gamma = 1.386$ (same as theoretical 3D Heisenberg model). The obtained values are substituted in Eq. (7) to generate a MAP. Figure 1a–d shows the MAP for the respective alloys at different temperatures. From the linear extrapolation of isotherms, the intercept on $M^{1/\beta}$ and $H/M^{1/\gamma}$ axis provide the value of $(M_S)^{1/\beta}$ and $(\chi_0^{-1})^{1/\gamma}$, respectively. The $M_S(T)$ and $\chi_0^{-1}(T)$ values thus obtained, are utilized to fit in Eq. (1) and Eq. (2), respectively. According to these equations, the new values of β and γ can be obtained from the slope of $\log(M_S)$ vs $\log(\varepsilon)$ and $\log(\chi_0^{-1})$ vs $\log(\varepsilon)$, respectively. It is important to note that during the straight-line fitting, T_C is adjusted in Eq. (1) and Eq. (2) such that a best fit can be obtained. Hence, to construct the new MAP, the new values of β and γ are re-used. Furthermore, to obtain the stable values of β , γ , and T_C (as listed in Table 1), this process is repeated. Using this method, for each alloy, a set of parallel isotherms has been generated. The final obtained values of $\chi_0^{-1}(T)$ and $M_S(T)$ are again used to estimate the values of critical exponents and T_C through scaling law. Here, for each alloy, $M_S(T)$ and $\chi_0^{-1}(T)$ are represented as a function of temperature as shown in Fig. 2a–d. Using these values of $M_S(T)$ and

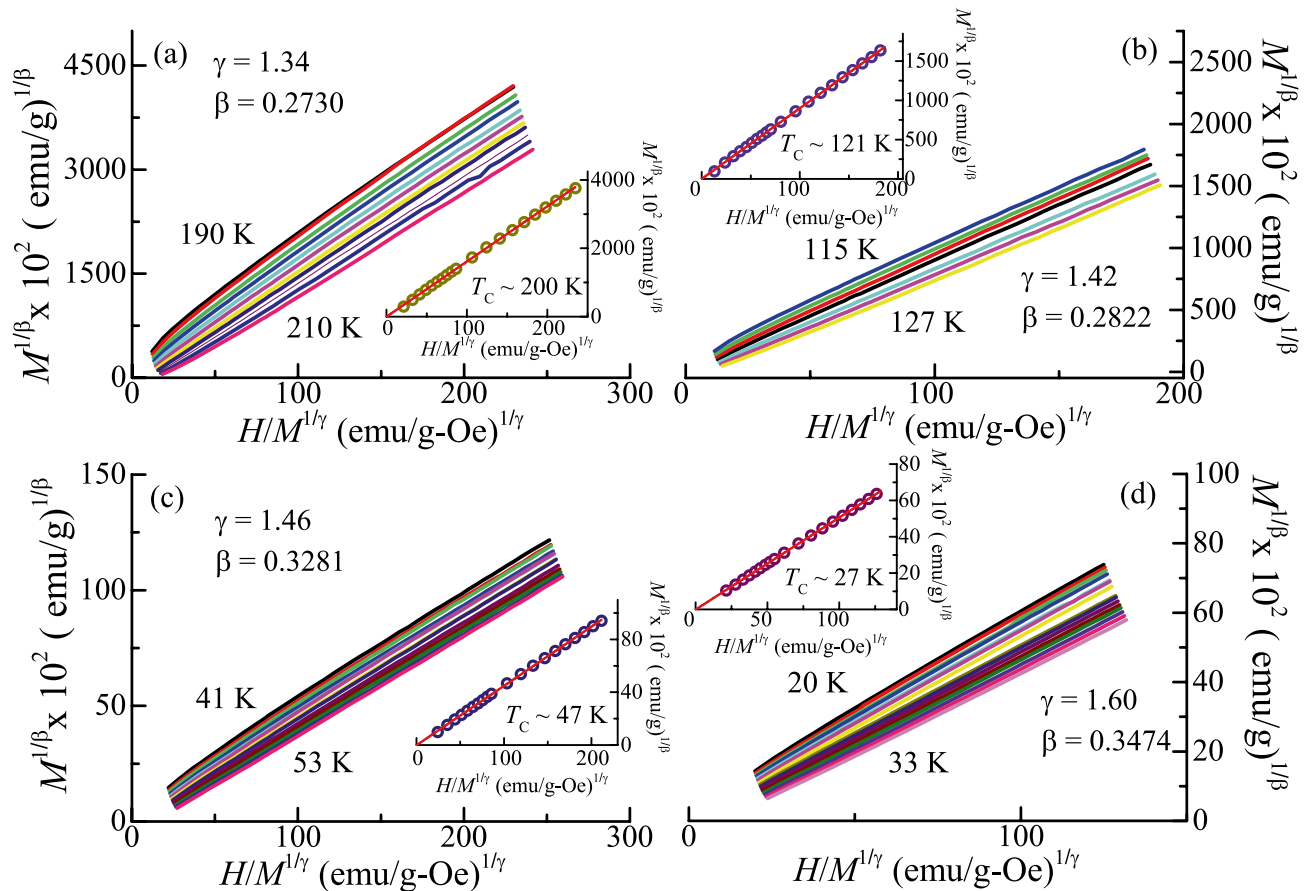


Figure 1. MAP ($M^{1/\beta}$ vs $H/M^{1/\gamma}$) of (a) Fe_2CrAl , (b) $\text{Fe}_{1.75}\text{Mn}_{0.25}\text{CrAl}$, (c) $\text{Fe}_{1.5}\text{Mn}_{0.5}\text{CrAl}$, and (d) $\text{Fe}_{1.25}\text{Mn}_{0.75}\text{CrAl}$ with estimated critical exponents (as also listed in Table 1). Insets: MAP of each alloy at T_C . Red line: Linear fitting of isotherm at T_C .

$\chi_0^{-1}(T)$, the finally obtained values of critical exponents and T_C are listed in Table 1. As inferred from Table 1, the estimated values from both methods (scaling law and MAP) match well with each other.

For the exact determination of critical exponents along with T_C , $M_S(T)$, and $\chi_0^{-1}(T)$, the data is analysed using a Kouvel-Fisher (KF) plot³⁰. In this method, $M_S(dM_S/dT)^{-1}$ vs T and $\chi_0^{-1}(d\chi_0^{-1}/dT)^{-1}$ vs T give a linear fit with slopes $1/\beta$ and $1/\gamma$, respectively. From these plots, T_C can be easily obtained from the intercept of the fitted straight lines. KF plots for all alloys have been presented in Fig. 3a–d. The estimated exponents and T_C are listed in Table 1. The tabulated values of critical exponents and T_C estimated through KF plot and MAP matches reasonably well.

$M(H, T_C)$ vs H isotherms for each alloy are plotted as shown in the supplementary material Fig. S2a–d, where insets represent the same plot in log–log scale. The log M vs log H curve will show a linear variation with slope $1/\delta$ (according to Eq. 3). The values of δ are determined from straight-line fitting. The exponent δ is estimated from the Widom-scaling relation³¹

$$\delta = 1 + \frac{\gamma}{\beta} \quad (8)$$

using the value of γ and β obtained from MAP studies. The obtained values of δ are 5.69 ± 0.08 , 5.94 ± 0.05 , 5.28 ± 0.08 , and 5.56 ± 0.01 for $x = 0.0, 0.25, 0.5$, and 0.75 compositions. These values are very near to the value estimated from the $M(H, T_C)$ vs H curve. Hence, in the present study, the estimated critical exponents are accurate and do not contradict with each other. All the critical exponents estimated from different methods along with the theoretical values are given in Table 1.

It is noted that the experimentally estimated critical exponents in our case do not lie within any conventional universality models. Hence, to confirm whether the obtained parameters can produce the scaling equation of state (Eq. 5), the scaled m as a function of scaled h for each alloy is shown in Fig. 4a–d. Inset of the Fig. 4a–d represents the log–log scale of the same plot. It can be clearly observed that the scaling law is satisfied in each case. All the generated isotherms diverge into two different curves: one above and one below T_C . Furthermore, the consistency of the critical exponents and T_C has been re-checked using more meticulous method where m^2 is represented as function of h/m ³² as shown in the supplementary information Fig. S3a–d. For each alloy, as expected, it is observed that the data fall into two separate branches.

Composition	Ref	Method	β	T_C (M ₀) K	γ	T_C (χ_0) K	δ	T_C^{17}
Fe ₂ CrAl	This work	MAP	0.2730	201.89 ± 0.37	1.34	201.11 ± 0.14	5.91	202 K
		KF plot	0.273 ± 0.01	201.06 ± 0.04	1.35 ± 0.02	201.01 ± 0.03	5.94 ± 0.03	
		CI	–	–	–	–	5.69 ± 0.08	
Fe _{1.75} Mn _{0.25} CrAl	This work	MAP	0.2822	120.90 ± 0.05	1.42	121.19 ± 0.06	6.03	120 K
		KF plot	0.282 ± 0.02	120.34 ± 0.09	1.41 ± 0.03	121.02 ± 0.02	6 ± 0.01	
		CI	–	–	–	–	5.94 ± 0.05	
Fe _{1.5} Mn _{0.5} CrAl	This work	MAP	0.3281	48.6 ± 0.25	1.46	47.32 ± 0.05	5.45	48 K
		KF plot	0.326 ± 0.02	46.67 ± 0.01	1.47 ± 0.05	47.41 ± 0.01	5.45 ± 0.02	
		CI	–	–	–	–	5.28 ± 0.08	
Fe _{1.25} Mn _{0.75} CrAl	This work	MAP	0.3474	26.86 ± 0.09	1.6	27.15 ± 0.05	5.61	27 K
		KF plot	0.345 ± 0.13	26.79 ± 0.06	1.61 ± 0.04	27.10 ± 0.04	5.60 ± 0.07	
		CI	–	–	–	–	5.56 ± 0.01	
Co ₅₀ Cr ₂₅ Al ₂₅	13	MAP	0.488 (3)		1.144 (4)		3.336 (5)	
		KF Plot	0.482 (13)		1.148 (16)		3.382(20)	
		CI					3.401(4)	
Co ₄₅ Ni ₅ Cr ₂₅ Al ₄₅	13	MAP	0.513(7)		1.048(4)		3.043 (7)	
		KF plot	0.511(7)		1.028 (6)		3.012(8)	
		CI					2.976 (11)	
Co ₂ TiGe	16	MAP	0.495		1.325		3.677	
		KF plot	0.495		1.324(4)		3.675	
		CI					3.671(1)	
Mean field theory	32	Theory	0.5		1		3	
3D Heisenberg model (O*)	32	Theory	0.365		1.386		4.80	
3D Heisenberg model (D*)	39	Theory	0.5		2		5	
3D Ising model	32	Theory	0.325		1.241		4.82	
3D XY model	32	Theory	0.346		1.316		4.81	

Table 1. Values of the exponents β , γ , and δ as determined from the modified Arrott plot, Kouvel-Fischer plot and critical isotherm for Fe₂CrAl, Fe_{1.75}Mn_{0.25}CrAl, Fe_{1.5}Mn_{0.5}CrAl, and Fe_{1.25}Mn_{0.75}CrAl. The theoretically predicted values for various universality classes are also listed for comparison. *O ordered, D disordered.

As the critical exponents obtained from various methods do not fall in any universality class, it is important to determine whether the values of γ and β match with any universal model under the asymptotic limit. Hence, we have estimated the effective critical parameters as a function of ϵ . It can be observed from the Fig. 5a–d that both parameters exhibit non-monotonic change with variation in ϵ . In case of Fe₂CrAl, it can also be seen that β_{eff} and γ_{eff} show a slight dip (at $\epsilon = -0.02$) and a peak (at $\epsilon = 0.05$) before approaching the asymptotic limit ($\epsilon \rightarrow 0$). A similar trend in β_{eff} and γ_{eff} for other compositions is observed. Here, the values of β_{eff} and γ_{eff} at ϵ_{min} do not match with any conventional universal model. Additionally, the data do not completely fall into two distinct branches, with values of β_{eff} and γ_{eff} estimated at ϵ_{min} . This can be due to the following reasons: (i) ϵ_{min} does not lie in the asymptotic region and T_C must be considered more closely for asymptotic parameters or (ii) ϵ_{min} lies in the asymptotic regime; a similar type of disagreement of effective critical exponents (with any universal model) is also noted for other disordered materials^{33,34}. In case of crystalline FM, $\gamma_{\text{eff}}(\epsilon)$ shows a monotonic decrement with an increment in ϵ , whereas a peak is observed in amorphous FM³². From Fig. 5a–d, it is noted that the temperature variation of the effective critical exponents is similar to the behaviour seen in disordered FM. Thus, the above observations signify the influence of disorder on the critical exponent's values. In Fe_{2-x}Mn_xCrAl, there is a presence of anti-site disorder between Fe and Al, which has been reported in detail in Ref.²³. This disorder also increases with the Mn content and results in the formation of inhomogeneous magnetic phase. Hence, unconventional values of critical exponents are observed in Fe_{2-x}Mn_xCrAl.

Discussions

In recent years, critical phenomenon is widely studied in Heusler alloys^{7–17}. It has been found that the obtained values of critical exponents usually fall into a distinct universality class. For example, in Co₂CrAl and Co₅₀Ni₅Cr₂₅Al₂₅ the critical exponent values (given in Table 1) are almost similar to the value as predicted by mean field model¹³. This explains the presence of long-range FM interactions in these alloys. However, the critical exponents noted for Fe_{2-x}Mn_xCrAl are unconventional and do not belong to any universality class. In our previous studies, it is reported that Fe₂CrAl undergoes FM to PM transition around $T_C \sim 202$ K with the presence

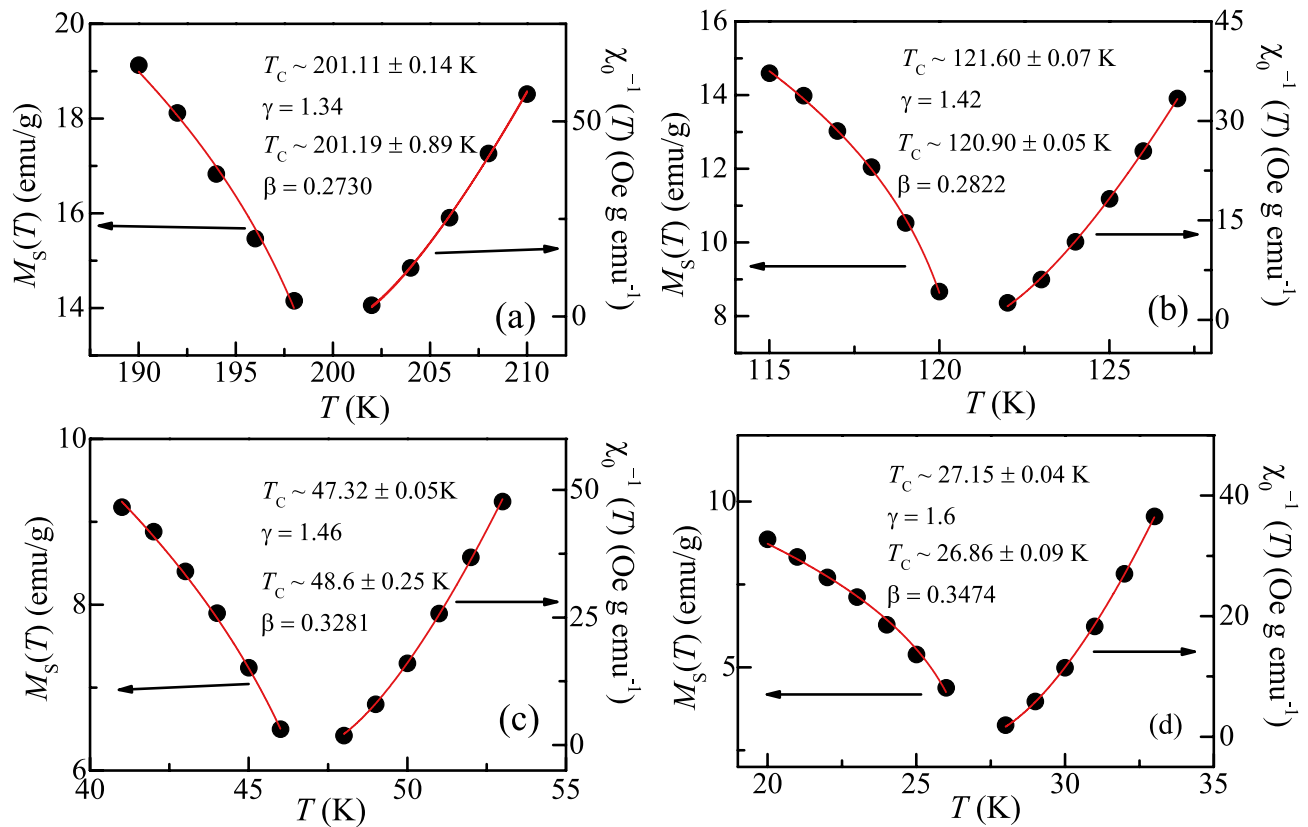


Figure 2. Temperature response of $M_S(T)$ and $\chi_0^{-1}(T)$ of (a) Fe_2CrAl , (b) $\text{Fe}_{1.75}\text{Mn}_{0.25}\text{CrAl}$, (c) $\text{Fe}_{1.5}\text{Mn}_{0.5}\text{CrAl}$, and (d) $\text{Fe}_{1.25}\text{Mn}_{0.75}\text{CrAl}$. The critical exponents and T_C are obtained from fitting of Eqs. (1) and (2).

of GP above T_C . With increment in Mn concentration, T_C decreases, and the temperature regime between FM and GP increases as shown in the phase diagram²³. In the present study, we have noted that the values of T_C (corresponding to each alloy) obtained through various techniques matches reasonably well with the previous reported values²³. The value of γ for the parent alloy is found to be 1.34 which is near to that reported for an ordered 3D Heisenberg model. This value increases with increasing Mn-concentration and is found to be 1.6 for $\text{Fe}_{1.25}\text{Mn}_{0.75}\text{CrAl}$. It is similar to that reported for a disordered 3D Heisenberg model. Physically, γ represents the degree of divergence of $\chi(T)$ at T_C , smaller the value of γ , sharper will be the divergence. For the parent alloy, γ is smaller as compared to $\text{Fe}_{1.25}\text{Mn}_{0.75}\text{CrAl}$, which is in accordance to the observation of the sharp transition in the former case. Also, the larger magnitude of γ indicates the broader temperature range of PM-FM transition. The observed trend in the value of γ is consistent with the increment of temperature regime of GP. The Yang-Lee theory²¹ of phase transition predicts that the singularity of the GP can lead to unusual critical behaviour i.e., a discontinuity in the $M(H)$ at $T = T_C$. It is reflected in observed larger values of critical exponent δ . In the present case, unusual larger values of δ are noted for these alloys. This behaviour suggests that the GP affects γ and δ . As reported in Ref.²³, because of anti-site disorder, GP arises in these alloys. Interestingly, the observed non-monotonic temperature variation of γ_{eff} also reflects the effect of disorder on the critical exponents. Here, it can be conjectured that the presence of random anti-site disorder can lead to the broader distribution of the local exchange fields due to the competition between AFM and FM exchange interactions. Similar behaviour was also noted in $\text{Fe}_{100-x}\text{Pt}_x$ alloy, where the value of critical exponent γ was enhanced due to the increment in the metallurgical site disorder³³.

In Fe_2CrAl , it is observed that there is a presence of CGP regime in the low temperature regime (below T_C). This regime increases with increasing Mn-substitution. For Fe_2CrAl , the value of β is 0.273, which does not belong to any universality class. With increment in Mn content, the value of β increases and approaches ordered 3D Heisenberg model, as found for $\text{Fe}_{1.25}\text{Mn}_{0.75}\text{CrAl}$ ($\beta = 0.347$). Physically, β represents the growth of spontaneous magnetization below T_C , i.e., smaller value indicates faster growth. In the present case, the value of β is smaller for the parent alloy as compared to $\text{Fe}_{1.25}\text{Mn}_{0.75}\text{CrAl}$, implying that the growth of M_S is faster in the former alloy. With Mn substitution, the rate of growth decreases near T_C , which is a consequence of increased CGP region.

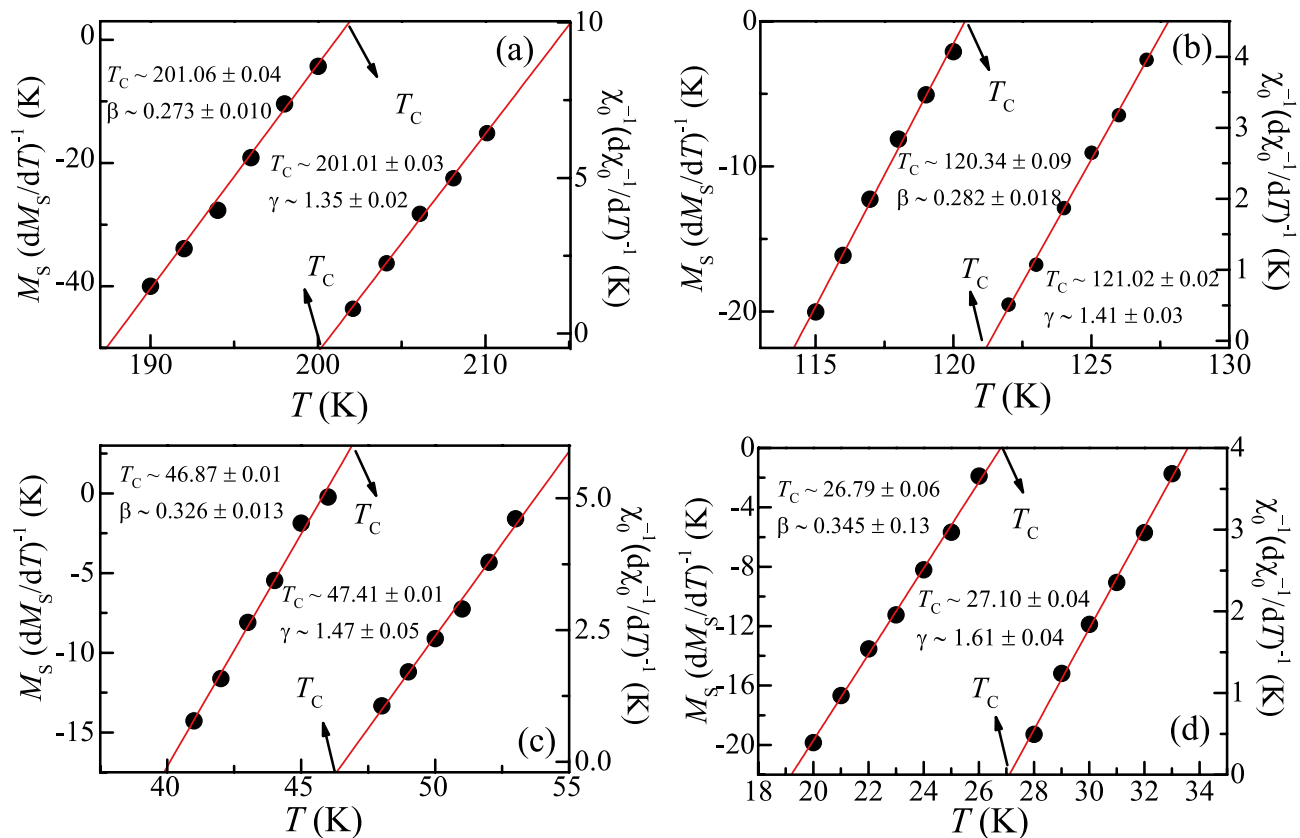


Figure 3. Temperature dependent M_S (dM_S/dT)⁻¹ (left axis) and $\chi_0^{-1}(d\chi_0^{-1}/dT)^{-1}$ (right axis) of (a) Fe₂CrAl, (b) Fe_{1.75}Mn_{0.25}CrAl, (c) Fe_{1.5}Mn_{0.5}CrAl, and (d) Fe_{1.25}Mn_{0.75}CrAl. Solid red lines denote the linear fitting.

However, the obtained values of β ($=0.273$) for Fe₂CrAl in our case does not match well with the earlier reported value of β ($=0.42$) for the same alloy³⁵. This discrepancy in the obtained value of β can arise due to presence of short-range correlations (in CGP) below T_C in our case and has not been reported in the latter case.

Hence, it can be said that critical exponents for disordered ferromagnetic systems is not in accordance with any conventional universality classes. Both γ and β are affected due to the presence of GP and CGP, respectively. The unconventional behaviour of critical exponents is not unusual and has also been observed in various alloys as well as oxides. For example, a large value of β ($=0.43$) is found due to phase segregation in La_{1-x}Sr_xCoO₃ compound³⁶. Similarly, Gd₈₀Au₂₀ exhibits unconventional exponents $\beta=0.44$ and $\gamma=1.29$, which arises due to spin dilution on non-magnetic ion substitution³⁷. Interestingly, due to presence of GP in La_{0.79}Ca_{0.21}MnO₃, larger values of γ and δ are observed²¹. Similarly, in the case of Co₂TiGe γ and δ deviate from the 3D Heisenberg model¹⁶. The obtained values of these exponents (listed in Table 1) reflect the presence of sizable critical spin fluctuations. This is observed due to the existence of magnetic inhomogeneity in the alloy. Thus, our results imply that critical phenomenon in Fe_{2-x}Mn_xCrAl cannot be described based on the existing universal class models.

Conclusion

The influence of CGP and GP on the critical exponents near the PM-FM phase transition of Fe_{2-x}Mn_xCrAl ($0 \leq x < 1$) has been investigated. Each alloy exhibits a SOPT. The obtained critical exponents from different methods match well with each other. For Fe₂CrAl, the estimated value of β is smaller than in the ordered 3D Heisenberg model, whereas γ is found to be near to this model. Along the series, both exponents β and γ show an increasing trend. For all alloys, the temperature dependences of γ_{eff} and β_{eff} resemble disordered ferromagnets, signifying the effect of anti-site disorder. This disorder induces Griffiths phase-like properties above T_C , which is reflected by the unconventionally larger values of γ and δ . Additionally, the observed trend in β can be attributed to increment in CGP regime due to Mn-substitution. Our study will be helpful to comprehend the effect of inhomogeneous magnetic phases (above and below T_C) on the critical behaviour of weak ferromagnetic Heusler alloys.

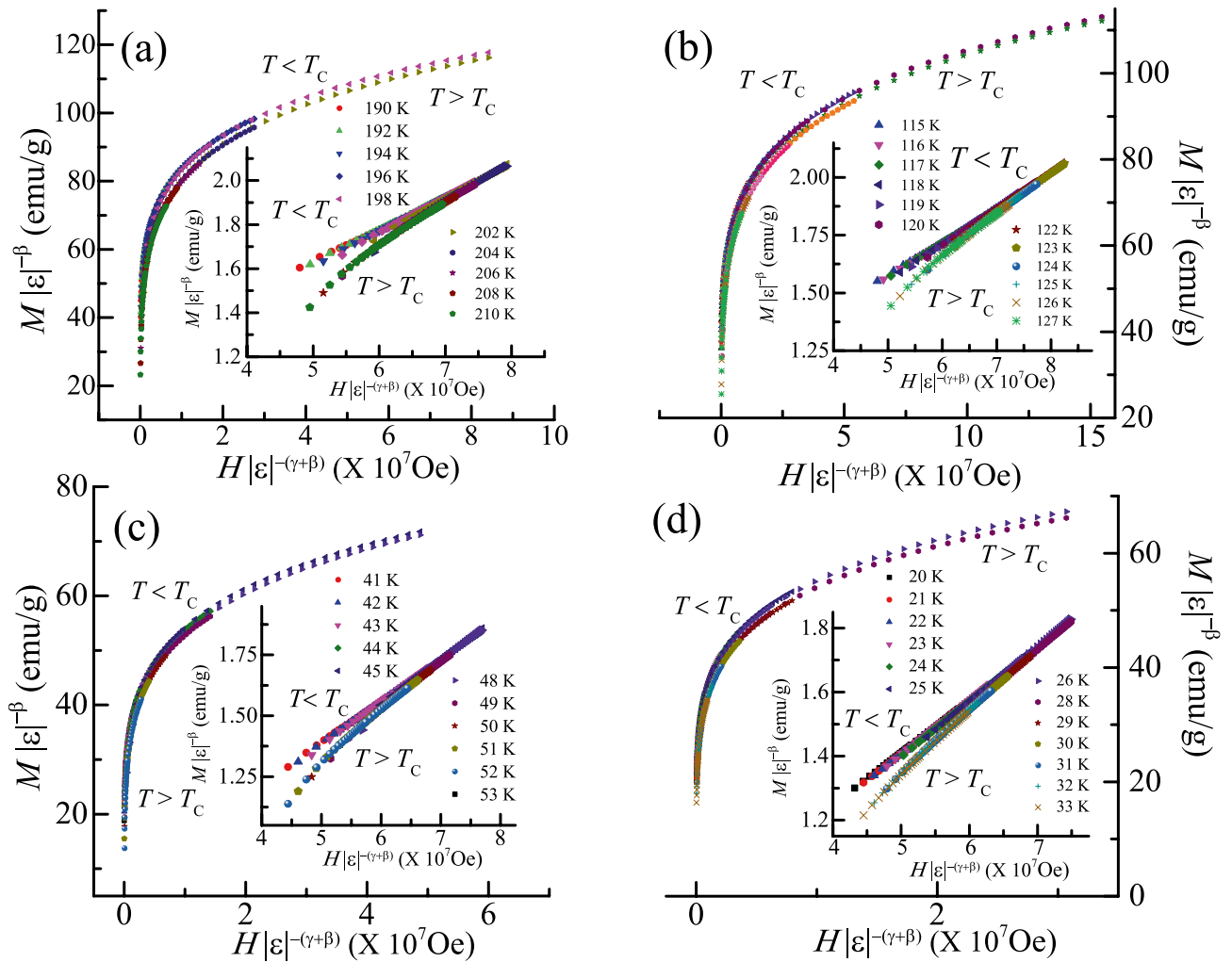


Figure 4. Renormalized m as a function of renormalized h (Eq. 5) with critical exponents and T_C from the Table 1 for (a) Fe_2CrAl (b) $\text{Fe}_{1.75}\text{Mn}_{0.25}\text{CrAl}$ (c) $\text{Fe}_{1.5}\text{Mn}_{0.5}\text{CrAl}$ and (d) $\text{Fe}_{1.25}\text{Mn}_{0.75}\text{CrAl}$. Insets: m vs h in the log–log scale.

Methods

The series of alloys, $\text{Fe}_{2-x}\text{Mn}_x\text{CrAl}$ ($x = 0, 0.25, 0.5, \text{ and } 0.75$) are the same as those reported in Ref.²³. Structural characterization of these alloys has been already reported in Ref.²³. From that study, we have concluded the existence of anti-site disorder in all studied alloys. Also, an increment in anti-site disorder with Mn content was also noted. Additionally, in Ref.³⁸, morphological and compositional analysis of all these alloys has been carried out. It confirms the homogenous distribution of all elements in the respective alloys, which also indicates that the disorder is evenly distributed. Magnetic field (H) dependent magnetization (M) measurements have been done using Magnetic Property Measurement System (MPMS), Quantum Design, U.S.A. Rectangular shaped samples are used to obtain the M - H isotherms. The isotherms are collected in a close temperature interval (~ 1 K). Each isotherm is measured after cooling the sample from room temperature (and removal of the remanent magnetic field) to the measurement temperature. Before recording each isotherm, 10 min wait time has been given for proper stabilization of temperature.

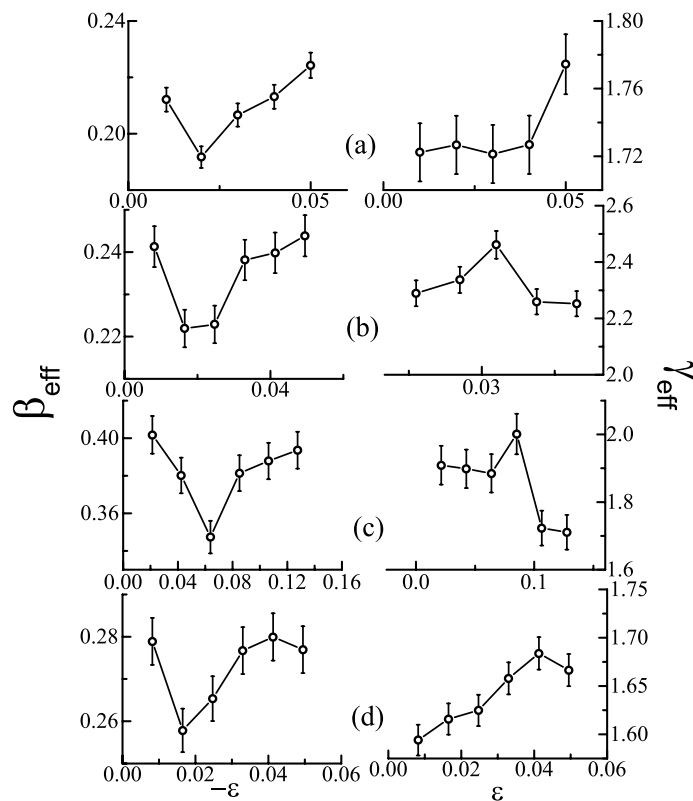


Figure 5. β_{eff} (left panel) and γ_{eff} (right panel) as a function of ϵ for ((a) Fe_2CrAl , (b) $\text{Fe}_{1.75}\text{Mn}_{0.25}\text{CrAl}$, (c) $\text{Fe}_{1.5}\text{Mn}_{0.5}\text{CrAl}$, and (d) $\text{Fe}_{1.25}\text{Mn}_{0.75}\text{CrAl}$.

Received: 29 July 2021; Accepted: 7 September 2021

Published online: 21 September 2021

References

- Heusler, F. Über magnetische Manganlegierungen. *Verh. Dtsch. Phys. Ges.* **5**, 219 (1903).
- Weber, J. Heusler alloys. *Contemp. Phys.* **10**, 559 (1969).
- Pierre, J. *et al.* Properties on request in semi-Heusler phases. *J. Alloys Compd.* **262**, 101–107 (1997).
- Tobole, J. & Pierre, J. Electronic phase diagram of the XTZ (X= Fe Co, Ni; T= Ti, V, Zr, Nb, Mn; Z= Sn, Sb) semi-Heusler compounds. *J. Alloys Compd.* **296**, 243 (2000).
- Graf, T., Felser, C. & Parkin, S. S. P. Simple rules for the understanding of Heusler compounds. *Prog. Solid State Chem.* **39**, 1–50 (2011).
- Saha, R., Srinivas, V. & Rao, T. V. Evolution of ferromagnetic like order in $\text{Fe}_2\text{V}_{1-x}\text{Cr}_x\text{Al}$ Heusler alloys. *Phys. Rev. B* **79**, 174423 (2009).
- Yadav, K. & Mukherjee, K. Effect of partial substitution of isovalent Mo at Cr-site on electronic structure and physical properties of Fe_2CrAl . *Intermetallics* **133**, 107153 (2021).
- Phan, T. L. *et al.* Coexistence of conventional and inverse magnetocaloric effects and critical behaviors in $\text{Ni}_{50}\text{Mn}_{50-x}\text{Sn}_x$ ($x= 13$ and 14) alloy ribbons. *Appl. Phys. Lett.* **101**, 212403 (2012).
- Zhang, P., Phan, T. L., Dan, N. H., Thanh, T. D. & Yu, S. C. Magnetocaloric and critical behavior in the austenitic phase of Gd-doped $\text{Ni}_{50}\text{Mn}_{37}\text{Sn}_{13}$ Heusler alloys. *J. Alloys Compd.* **615**, S335 (2014).
- Nan, W. Z. *et al.* Critical behavior near the ferromagnetic-paramagnetic transformation in the austenite phase of $\text{Ni}_{43}\text{Mn}_{46}\text{Sn}_8\text{X}_3$ (X= In and Cr) Heusler alloys. *J. Magn. Magn. Mater.* **443**, 171 (2017).
- Devarajan, U. *et al.* Coupled magnetocrystallographic transition in Ni-Mn-V-Ga Heusler alloys and its effect on the magnetocaloric and transport properties. *J. Phys. D: Appl. Phys.* **49**, 065001 (2016).
- Varzaneh, A. G. *et al.* Effect of Cu substitution on magnetocaloric and critical behavior in $\text{Ni}_{47}\text{Mn}_{40}\text{Sn}_{13-x}\text{Cu}_x$ alloys. *J. Alloys Compd.* **708**, 34 (2017).
- Panda, J., Saha, S. N. & Nath, T. K. Critical behavior and magnetocaloric effect in $\text{Co}_{50-x}\text{Ni}_x\text{Cr}_{25}\text{Al}_{25}$ ($x= 0$ and 5) full Heusler alloy system. *J. Alloys Compd.* **644**, 930 (2015).
- Nehla, P., Anand, V. K., Klemke, B., Lake, B. & Dhaka, R. S. Magnetocaloric properties and critical behavior of $\text{Co}_2\text{Cr}_{1-x}\text{Mn}_x\text{Al}$ Heusler alloys. *J. Appl. Phys.* **126**, 203903 (2019).
- Nehla, P. *et al.* Neutron diffraction and magnetic properties of $\text{Co}_2\text{Cr}_{1-x}\text{Ti}_x\text{Al}$ Heusler alloys. *Phys. Rev. B* **100**, 144444 (2019).
- Roy, S., Khan, N., Singha, R., Pariari, A. & Mandal, P. Complex exchange mechanism driven ferromagnetism in half-metallic Heusler Co_2TiGe : Evidence from critical behavior. *Phys. Rev. B* **99**, 214414 (2019).
- Saleheen, A. U. *et al.* Critical behavior in Ni_2MnGa and $\text{Ni}_2\text{Mn}_{0.85}\text{Cu}_{0.15}\text{Ga}$. *J. Appl. Phys.* **123**, 203904 (2018).
- Arumugam, S. *et al.* Structural, transport, magnetic, magnetocaloric properties and critical analysis of Ni-Co-Mn-Ga Heusler alloys. *J. Magn. Magn. Mater.* **442**, 460 (2017).
- Dash, S. *et al.* Impression of magnetic clusters, critical behavior and magnetocaloric effect in Fe_3Al alloys. *Phys. Chem. Chem. Phys.* **21**, 10823 (2019).
- Tarhouni, S. *et al.* Analysis based on scaling relations of critical behaviour at PM–FM phase transition and universal curve of magnetocaloric effect in selected Ag-doped manganites. *RSC Adv.* **8**, 18924–18307 (2018).

21. Jiang, W., Zhou, X., Williams, G., Mukovskii, Y. & Glazyrin, K. Is a Griffiths phase a prerequisite for colossal magnetoresistance?. *Phys. Rev. Lett.* **99**, 177203 (2007).
22. Rathi, A. *et al.* Signature of a Griffiths phase in layered canted antiferromagnet Sr₂IrO₄. *J. Mag. Mag. Mater.* **468**, 230 (2018).
23. Yadav, K., Sharma, M. K., Singh, S. & Mukherjee, K. Exotic magnetic behaviour and evidence of cluster glass and Griffiths like phase in Heusler alloys Fe_{2-x}Mn_xCrAl (0 ≤ x ≤ 1). *Sci. Rep.* **9**, 15888 (2019).
24. Stanley, H. E. *Introduction to phase transitions and critical phenomenon* (Oxford University Press, 1971).
25. Perumal, A., Srinivas, V., Rao, V. V. & Dunlap, R. A. Quenched disorder and the critical behavior of a partially frustrated system. *Phys. Rev. Lett.* **91**, 137202 (2003).
26. Srinath, S., Kaul, S. N. & Sostarich, M. K. Isotropic-Heisenberg to isotropic-dipolar crossover in amorphous ferromagnets with composition near the percolation threshold. *Phys. Rev. B* **62**, 11649 (2000) (**and references therein**).
27. Arrott, A. Criterion for ferromagnetism from observations of magnetic isotherms. *Phys. Rev.* **108**, 1394 (1957).
28. Banerjee, S. K. On a generalised approach to first and second order magnetic transitions. *Phys. Lett.* **12**, 16 (1964).
29. Arrott, A. & Noakes, J. E. Approximate equation of state for nickel near its critical temperature. *Phys. Rev. Lett.* **19**, 786 (1967).
30. Kouvel, J. S. & Fisher, M. E. Detailed magnetic behavior of nickel near its Curie point. *Phys. Rev.* **136**, A1626 (1964).
31. Widom, B. Equation of state in the neighborhood of the critical point. *J. Chem. Phys.* **43**, 3898 (1965).
32. Kaul, S. N. Static critical phenomena in ferromagnets with quenched disorder. *J. Mag. Mag. Mater.* **53**, 5 (1985).
33. Boxberg, O. & Westerholt, K. Critical exponents at the ferromagnetic phase transition of Fe_{100-x}Pt_x single crystals. *Phys. Rev. B* **50**, 13 (1994).
34. Dudka, M., Folk, R., Holovatch, Y. & Ivaneiko, D. Effective critical behaviour of diluted Heisenberg-like magnets. *J. Mag. Mag. Mater.* **256**, 243 (2003).
35. Saha, R., Srinivas, V. & Venimadhav, A. Observation of magnetic cluster phase above Curie temperature in Fe₂CrAl Heusler alloy. *J. Mag. Mag. Mater.* **324**, 1296 (2012).
36. Mira, J. *et al.* Critical exponents of the ferromagnetic-paramagnetic phase transition of La_{1-x}Sr_xCoO₃ (0.20 < x < 0.30). *Phys. Rev. B* **59**, 123 (1999).
37. Poon, S. J. & Durand, J. Critical phenomena and magnetic properties of an amorphous ferromagnet: Gadolinium-gold. *Phys. Rev. B* **16**, 316 (1977).
38. Yadav K., Singh S., Muthuswamy O., Takeuchi T., and Mukherjee K., Anomalous dependence of thermoelectric parameters on carrier concentration and electronic structure in Mn-substituted Fe₂CrAl Heusler alloy, cond-mat arXiv: 2006.03234 (2020).
39. Sobbotka, G. Critical phenomena of random spin systems: Second order ϵ -expansion. *J. Magn. Magn. Mater.* **28**, 1 (1982).

Acknowledgements

The authors acknowledge IIT Mandi for providing the experimental facilities and K.M. acknowledges the financial support from a research grant (Grant No. 03(1381)/16/EMR-II) from SERB, India.

Author contributions

K.Y. synthesized the alloys and performed the experiments. K.Y., D.R., and K.M. analyzed the data and wrote the manuscript.

Competing interests

The authors declare no competing interests.


Additional information

Supplementary Information The online version contains supplementary material available at <https://doi.org/10.1038/s41598-021-98377-y>.

Correspondence and requests for materials should be addressed to K.M.

Reprints and permissions information is available at www.nature.com/reprints.

Publisher's note Springer Nature remains neutral with regard to jurisdictional claims in published maps and institutional affiliations.

 **Open Access** This article is licensed under a Creative Commons Attribution 4.0 International License, which permits use, sharing, adaptation, distribution and reproduction in any medium or format, as long as you give appropriate credit to the original author(s) and the source, provide a link to the Creative Commons licence, and indicate if changes were made. The images or other third party material in this article are included in the article's Creative Commons licence, unless indicated otherwise in a credit line to the material. If material is not included in the article's Creative Commons licence and your intended use is not permitted by statutory regulation or exceeds the permitted use, you will need to obtain permission directly from the copyright holder. To view a copy of this licence, visit <http://creativecommons.org/licenses/by/4.0/>.

© The Author(s) 2021